JOURNAL OF GEOPHYSICAL RESEARCH, VOL. 114, F03011, doi:10.1029/2008JF001173, 2009

Snow and ice facies variability and ice layer formation on Canadian Arctic ice caps, 1999–2005

Gabriel J. Wolken,[1] Martin Sharp,[1] and Libo Wang[2]

Received 10 October 2008; revised 9 March 2009; accepted 2 June 2009; published 21 August 2009.

[1] Time series of enhanced resolution data from the SeaWinds scatterometer aboard QuikScat were used to map the distribution of snow and ice surface facies and ice layer formation in the percolation zone on ice caps in the Queen Elizabeth Islands during the period 1999–2005. Iterative Self-Organizing Data Analysis classification of the mean postfreeze-up biweekly average σ^0 signal for the 7-year period resulted in the delineation of four snow and ice surface facies (interpreted as the percolation, saturation, superimposed ice, and glacier ice zones). Analysis with National Centers for Environmental Prediction/National Center for Atmospheric Research Reanalysis reveals that changes in geopotential height in the troposphere (700, 500, and 300 hPa) and air temperature (700 hPa level) are positively (negatively) correlated with area changes in the glacier ice (percolation and saturation) zones and changes in facies boundary elevation. The change in biweekly-averaged backscatter following the freeze-up periods between successive autumns was used to map changes in the distribution of ice layers formed by meltwater percolation and refreezing in the snowpack within the percolation zone. Strongly positive air temperature anomalies at the 700 hPa level in 2001 and 2005 are consistent with extensive ice layer formation in the percolation zones of all ice caps. Such large interannual changes in ice layer formation are likely associated with large changes to the density profile of the snowpack and may be associated with surface elevation changes that are unrelated to changes in surface mass balance.

Citation: Wolken, G. J., M. Sharp, and L. Wang (2009), Snow and ice facies variability and ice layer formation on Canadian Arctic ice caps, 1999–2005, *J. Geophys. Res.*, *114*, F03011, doi:10.1029/2008JF001173.

1. Introduction

[2] Polar ice masses play a critical role in regulating both regional and global climate and are sensitive indicators of climate change. Over the last century (1906–2005), global average surface air temperatures have risen by ~0.74°C and average Arctic temperatures have increased at nearly double that rate, resulting in a substantial reduction in both land and sea ice cover [*Trenberth et al.*, 2007]. One of the key global concerns with rising Arctic temperatures is the continued melting of terrestrial ice masses and the subsequent rise in global sea level [*Hassol*, 2004; *Kaser et al.*, 2006; *Trenberth et al.*, 2007; *Meier et al.*, 2007]. Although the potential contribution to sea level rise from ice sheets is greater than that from ice caps and glaciers, the latter may be more sensitive and respond more rapidly to changes in climate [*Raper and Braithwaite*, 2006; *Meier et al.*, 2007]. Hence, given the likely increase in Arctic temperature and the potential for increases in rates of sea level rise resulting from anthropogenic climate change, it is crucial that we increase our knowledge of the mass balance of Arctic glaciers and ice caps and continue to monitor their behavior.

[3] Ice caps in Arctic Canada represent the largest ice covered area on earth outside Greenland and Antarctica, totaling ~28% of the area of all glaciers and ice caps [*Dyurgerov and Meier*, 2005]. Most of the glaciers and ice caps in Arctic Canada are in the Queen Elizabeth Islands (QEI), where the ice covered area is over 110,000 km^2 (Figure 1 [*Koerner*, 2002]). Given the remoteness of polar regions, however, field-based mass balance measurements are sparse, typically of short duration, and biased toward smaller ice masses [*Dyurgerov and Meier*, 2005]. Most regional scale mass balance estimates are derived from either modeling or extrapolation of the few available mass balance measurements [*Zuo and Oerlemans*, 1997; *Kaser et al.*, 2006]. It is not known whether these approaches provide reliable estimates of the surface mass balance for an array of geographically and topographically diverse ice masses of widely varying sizes.

[4] Regional assessments of ice sheet and ice cap mass balance can, in principle, be obtained by measuring changes in their surface elevations over time with either airborne [*Krabill et al.*, 2002; *Thomas et al.*, 2003; *Abdalati et al.*, 2004] or satellite [*Zwally et al.*, 2002; *Davis et al.*, 1998] altimeters. However, the accuracy of such mass balance

[1]Department of Earth and Atmospheric Sciences, University of Alberta, Edmonton, Alberta, Canada.
[2]Climate Research Division, Atmospheric Science and Technology Directorate, Environment Canada, Toronto, Ontario, Canada.

0148-0227/09/2008JF001173$09.00

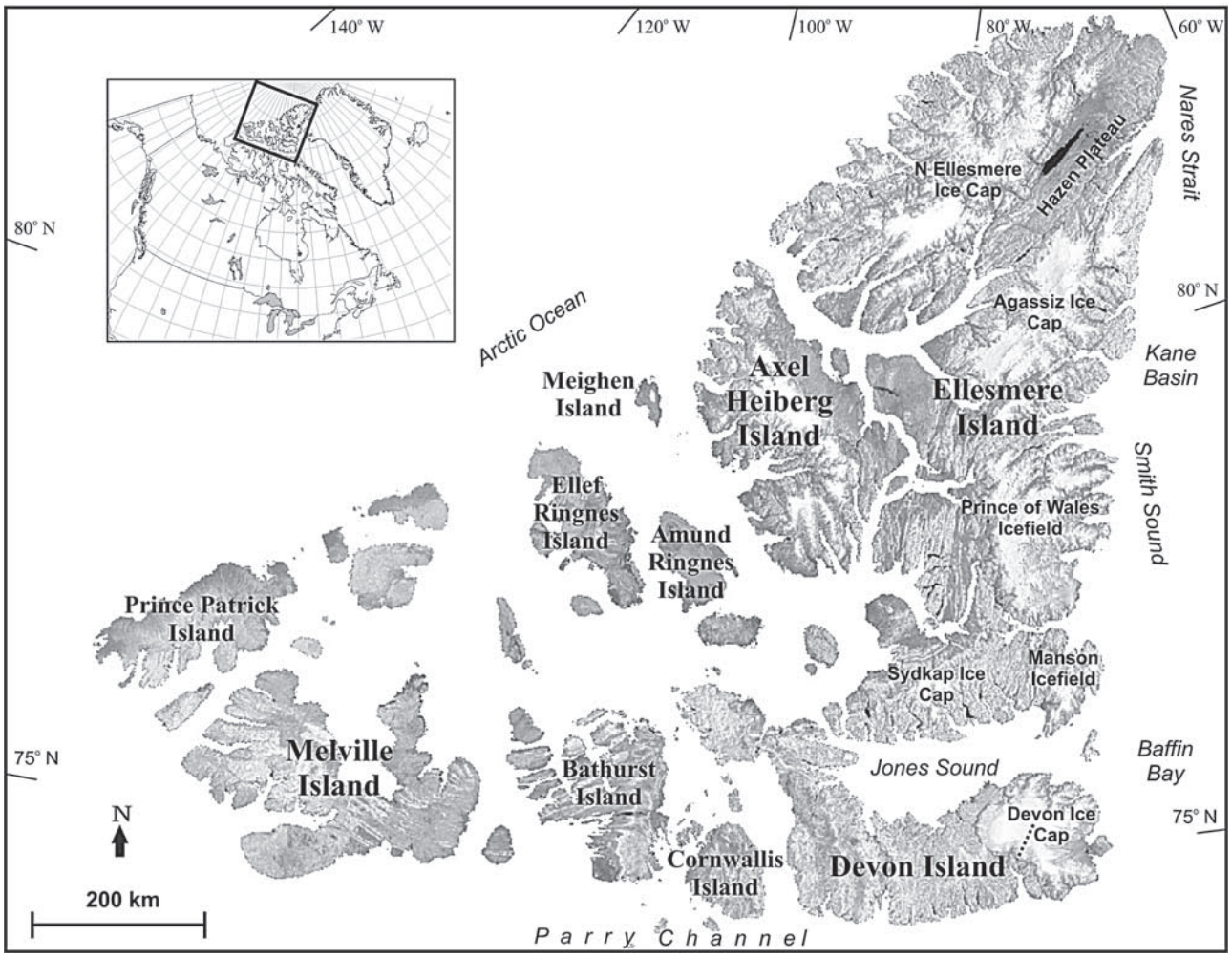

Figure 1. Map of the major ice caps and ice fields in the Queen Elizabeth Islands, Arctic Canada.

estimates is highly dependent on knowledge of spatiotemporal variations in near surface firn density [*Braithwaite et al.*, 1994]. Rates of firn densification are strongly affected by the extent of meltwater percolation into subsurface snow and firn, which can result in refreezing and ice layer formation. A slight change in summer melt can have a significant influence on the density profile of near surface snow and firn, and hence the thickness of the annually accreted firn layer, even in the absence of a change in surface mass balance. Thus, in order to correctly interpret a measured elevation change, it is necessary to evaluate the distribution of snow and ice surface facies, and the relative contributions to elevation change arising from variability in snow/firn densification rates and changes in mass balance. An additional challenge associated with interpreting radar altimeter measurements of surface elevation change is isolating the source of the dominant backscatter signal from the snow/firn medium and its relationship to the true surface of the ice mass. The source of backscatter is often unknown because of the presence of inhomogeneities (e.g., ice layers, lenses, pipes, and granules) in the snow/firn layer between the ice surface and the previous year's end of summer snow surface [*Wingham*, 1995; *Legresy and Remy*, 1997; *Scott et al.*, 2006]. Interannual changes in the location of the mean reflecting horizon relative to the true ice surface arising from changes in snow/firn stratigraphy and facies zone boundaries can potentially generate spurious changes in surface height as measured by radar altimeters [*Thomas et al.*, 2008].

[5] Snow and ice facies distributions are sensitive to changes in the annual processes of accumulation and surface melt. Monitoring the spatial variability in snow and ice surface facies on ice caps/sheets can improve our understanding of surface albedo variations and associated temperature and mass balance feedback mechanisms and provide valuable information about trends in regional mass balance. In this paper, we present maps of the distribution of snow and ice facies on the largest ice caps/fields in the QEI (Devon Island ice cap, Sydkap, Manson Icefield, Prince of Wales Icefield (POW), Agassiz Ice Cap, N Ellesmere Island, and Axel Heiberg Island) during the period 1999–2005 derived from enhanced resolution QuikSCAT (QS) scatterometer data [*Long and Hicks*, 2005]. We present analyses of facies changes over the 7-year period and evaluate the interannual variability in end of summer ice layer formation over QEI ice caps, which allows for the identification of areas where firn densification rates may have changed between years and thus, where radar altimeter measure-

ments may suggest spurious changes in surface elevation and mass balance.

2. Background: Snow and Ice Surface Facies and Previous Work

[6] Distinct altitudinally organized zones or "facies" of snow and ice characterize the surface of glaciers, ice caps, and ice sheets. These facies are delineated on the basis of their distinct surface and near-surface physical properties, which are related to patterns in the extent and magnitude of summer melt [*Benson*, 1962; *Long and Drinkwater*, 1994]. These patterns are most strongly associated with elevation and, to a lesser extent, proximity to open water [*Massom and Lubin*, 2006]. The different snow and ice facies are separated by transitional zones in which snow and firn with the physical characteristics of both neighboring facies can be present.

[7] All snow and ice facies can be found on ice caps in the QEI, but they are most completely developed on the Greenland Ice Sheet, where they were first investigated by *Benson* [1962]. At the highest elevation, the dry snow zone represents an area with no summer melt. The dry snowline separates the dry snow zone from the percolation zone. In the percolation zone, surface meltwater percolates into the snowpack and refreezes, forming ice layers, pipes and lenses. The lower boundary of the percolation zone is referred to as the saturation line, which marks the upper limit of the saturation zone. The saturation zone (or wet snow zone) represents an area of the ice cap/sheet where the temperature of the entire snowpack was raised to the melting point at some time during the melt season. The lower boundary of the saturation zone is referred to as the snow/firn line, which also defines the upper boundary of the superimposed ice zone. The superimposed ice zone represents the lowest part of the accumulation area and is a transitional zone in which ice accretes by the refreezing of meltwater to the glacier ice surface. The equilibrium line is located at the lower boundary of this zone and it connects all points at which the annual net balance is zero. The altitude of this line is referred to as the equilibrium line altitude (ELA). The glacier ice zone corresponds to the ablation area, in which summer melt removes the entire annual snow accumulation and exposes glacier ice.

[8] Snow and ice surface facies were originally monitored using in situ data collected from mass balance transects. Remote sensing of snow and ice surface facies began with the use of optical sensors [*Østrem*, 1975], but mapping of snow and firn facies using optical remote sensing has had limited success [*Nolin and Payne*, 2007]. Many studies have concluded that the visible and near infrared wavelengths are inappropriate for delineating facies because the boundaries are indistinguishable because of shallow or nonexistent gradients between zones [*Williams et al.*, 1991; *Greuell and Knap*, 2000; *Bindschadler et al.*, 2001]. Additionally, facies mapping with optical sensors is often precluded by environmental factors such as persistent cloud cover or fresh snow [*Hall et al.*, 1987]. Microwave radiation is sensitive to surface and subsurface physical properties of snow and ice and is not affected by the usual environmental factors that prevent facies mapping with optical sensors. A number of studies on Greenland [*Bindschadler and Vornberger*, 1992; *Fahnestock et al.*, 1993; *Jezek et al.*, 1993, 1994; *Long and Drinkwater*, 1994, 1999; Wismann and Boehnke 1996] and Antarctica [*Braun et al.*, 2000; *Bardel et al.*, 2002] have connected snow and ice facies to specific radar signatures derived from both synthetic aperture radar (SAR) and scatterometer data. SAR has also been used with some success in mapping superimposed and glacier ice facies on Svalbard [*Engeset et al.*, 2002; *Konig et al.*, 2002]. In Arctic Canada, however, snow and ice facies mapping has been limited to in situ measurements from only a few locations [*Koerner*, 1970].

[9] Ku-band scatterometers are effective at monitoring seasonally dependent changes in the radar backscatter cross section (σ^0) from ice sheets and ice caps [*Long and Drinkwater*, 1994, 1999]. Variations in backscatter are the result of metamorphic modifications of the surface and near-surface snow/ice through changes in the presence/absence of liquid water, snow grain size, surface roughness, or internal inhomogeneities such as ice layers. Snow and ice surface facies can be mapped on ice sheets using radar scatterometer data [e.g., *Long and Drinkwater*, 1999], but the resolution of scatterometer data is too low for facies mapping on ice caps. Enhanced resolution scatterometer products (see section 3.1 [*Long and Hicks*, 2005]), however, substantially increase the effective resolution of QS and allow for the regional scale mapping of snow and ice facies on ice caps in polar regions.

3. Methods

3.1. Data

[10] The Ku-band SeaWinds scatterometer on QS operates at a frequency of 13.4 GHz and has two constant incidence angles: 54° for the vertically polarized outer beam (1800 km swath) and 46° for the horizontally polarized inner beam (1400 km swath). Because QS has a wide swath and is a polar orbiting satellite, it can collect data from the polar regions several times daily with both ascending and descending passes, allowing the original data resolution (25 km^2) to be enhanced with the Scatterometer Image Reconstruction (SIR) algorithm [*Long et al.*, 1993; *Long and Hicks*, 2005]. From this algorithm, two forms of enhanced resolution QS backscatter (σ^0) images are created: egg and slice. SIR derived egg images are produced on a 4.5 km^2 grid while the slice images are produced on a 2.225 km^2 grid. Because of the lower incidence angle of horizontal polarization measurements, Ku-band backscatter from snow is higher in horizontal polarization than in vertical polarization [*Ulaby and Stiles*, 1981]. Thus, in this study we used horizontal polarization descending pass slice images to create time series of σ^0 over the QEI from 1999 (JD 200) to 2005 (JD 365).

[11] Interpretations of QS data and the results of analyses were validated using ground measurements of near surface air temperature, optical satellite imagery, and snow pit stratigraphy. Surface air temperature records were compiled from air temperature loggers deployed along transects on the Devon Island ice cap (Cryosat Transect) and POW [*Marshall et al.*, 2007; *Gardner and Sharp*, 2009] and used to validate QS melt detection. Optical satellite imagery (ASTER and Landsat) and snow pit stratigraphy from the Devon Cryosat transect in autumn 2004 (Figure 1 [*Bell et*

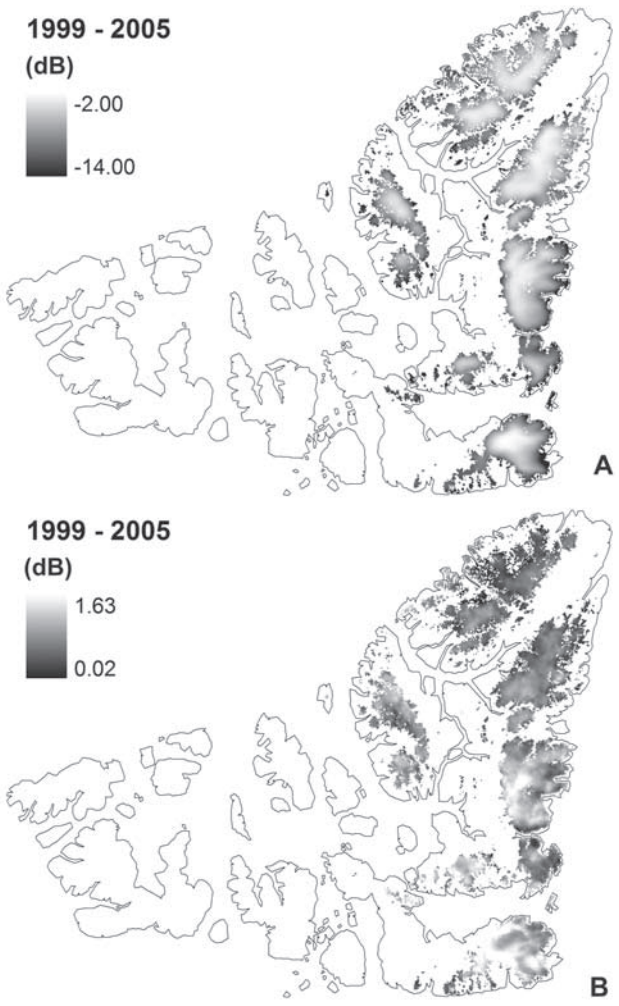

Figure 2. Seven-year (1999–2005) (a) average and (b) standard deviation of postfreeze-up biweekly-averaged σ^0 for each pixel on ice caps in the QEI.

al., 2008]) were used as a basis for interpreting postfreeze-up QS σ^0 signatures and validating facies classification results. Monthly mean geopotential height and tropospheric temperature data (1999–2005) were obtained from the National Centers for Environmental Prediction (NCEP)/National Center for Atmospheric Research (NCAR) Reanalysis (NNR) Project [*Kalnay et al.*, 1996].

3.2. Melt Mapping

[12] Annual melt onset and freeze-up dates and melt durations were calculated for each nonmixed pixel within the ice-covered areas of the QEI for the period 1999–2005 (following *Wang et al.* [2005]). The dramatic reduction in Ku-band σ^0 that occurs when liquid water appears at the surface or in the subsurface of the annual snowpack signifies the beginning of the melt season [*Ulaby and Stiles*, 1981]. Conversely, as melt ends and liquid water refreezes, an increase in backscatter occurs, indicating the end of the melt season. To detect melt onset and freeze-up in each pixel, *Wang et al.* [2005] used two dynamic thresholds based on winter (December–February) mean and standard deviation σ^0 values and empirically derived constants. The annual melt duration in each pixel was determined by calculating the number of days between melt onset and freeze-up dates minus the duration of any periods when melt was not detected (as indicated by short-term increases in σ^0). Melt durations derived from annual melt onset and freeze-up dates closely matched those derived from air temperature measurements, and were well correlated with the annual positive degree-day total [*Wang et al.*, 2005].

3.3. Classification of Snow and Ice Facies

[13] The postfreeze-up, biweekly-averaged σ^0 for each pixel was computed, beginning two weeks after the end of the melt season, for each year (1999–2005), and the average postfreeze-up biweekly-averaged σ^0 for the 7-year period was used to characterize the different snow and ice facies in the QEI. Classification of the snow and ice facies was performed using an Iterative Self-Organizing Data Analysis (ISODATA) technique. ISODATA is an unsupervised classification algorithm that iteratively assigns pixels to certain classes according to their proximity to class means [*Lillesand and Kiefer*, 1994]. The algorithm begins by arbitrarily defining clusters in the data space to which all pixels are assigned using minimum distance techniques. This step is followed by recalculation of cluster means and reassignment of pixels on the basis of the new means. This process continues through multiple iterations until the intracluster standard deviation is small and the intercluster standard deviation is large, allowing for the greatest separation between clusters. These final clusters represent the classes used to classify the data. The user specifies a range of classes for the given data set, but the classification algorithm defines the final number of classes. For the 1999–2005 mean postfreeze biweekly-averaged σ^0, the ISODATA classification algorithm was run for 30 iterations, with the acceptable number of classes specified to be within the range 4 to 10 and the class change threshold was set to 5%. The intraclass and interclass distances were set to 0.7 and 0.9 standard deviations, respectively.

4. Results and Discussion

4.1. Facies Classification

[14] The 7-year (1999–2005) average and standard deviation of the postfreeze-up biweekly-averaged σ^0 were calculated for each pixel on the QEI ice caps (Figure 2). ISODATA classification based on the average σ^0 resulted in four classes (Table 1 and Figure 3). Average backscatter values decrease with increasing class number and the classified image (Figure 3) reveals coherent, spatial patterns across all QEI ice caps that are highly and significantly ($p < 0.05$) correlated with elevation ($r = 0.78$) and consistent with autumn scatterometer signatures on the Greenland Ice Sheet [*Long and Drinkwater*, 1994, 1999].

[15] The four ISODATA classes were categorized as follows: 1. percolation zone; 2. saturation zone; 3. superimposed ice zone; 4. glacier ice zone. The dry snow zone is an intermittent feature on ice caps in the Canadian Arctic, and low annual snow accumulation fails to mask the high backscatter resulting from ice layers formed in previous summers. Hence, if a dry snow zone is present in a given year it is classified as part of the percolation zone. The dry

Table 1. Class Statistics Resulting From ISODATA Classification of the Average Postfreeze-Up Biweekly-Averaged σ^0 for the Period 1999–2005

Class	Minimum	Maximum	Mean	Standard Deviation
1	−4.03	−2.11	−3.19	0.49
2	−5.63	−4.04	−4.83	0.46
3	−6.90	−5.63	−6.23	0.36
4	−14.15	−6.90	−7.98	0.96

snow zone is, however, detectable in maps of the summer melt extent and duration [*Wang et al.*, 2005].

[16] Classification of postfreeze-up biweekly-averaged σ^0 was performed for each year (1999–2005) using the ISODATA classification procedures described above. Changes in the spatial distribution of snow and ice surface facies during the 1999–2005 period can be seen in Figure 4, and facies classification statistics are shown in Table 2. Field observations along the Cryosat transect in autumn 2004 [*Bell et al.*, 2008] confirm the interpretation of the percolation and saturation zones shown in the 2004 classified image (Figure 5). Average snowpack density in 2004 increases with decreasing elevation in the percolation zone. Snowpack data terminate at an elevation of ~1000 m, where thick and extensive ice layers precluded further snow pit excavation [*Bell et al.*, 2008], marking the upper boundary of the percolation-saturation zone transition (i.e., saturation line). Approximate facies boundaries in other years were checked against late summer optical satellite imagery (ASTER and Landsat).

4.2. Facies Distribution

[17] Previous studies used QS σ^0 to investigate melt processes on ice caps in the QEI [*Wang et al.*, 2005] and elsewhere in the Arctic [*Wang et al.*, 2007; *Sharp and Wang*, 2009], and analyzed interannual variability of melt parameters relative to the 2000–2004 climatological period. For consistency with those studies, this study also adopts the same pentad climatology for analyses of interannual variability in facies distribution (i.e., annual values are expressed as anomalies from the 2000–2004 climatology).

[18] The average facies distribution for the 2000–2004 pentad indicates that the glacier ice zone has the largest area, representing 27% of the total ice covered area (30,269 km^2) in the QEI (Table 3). The saturation zone has the next largest area (26%), followed by the percolation and superimposed ice zones (23.7 and 23.6%, respectively). Analysis of the distribution shows that the largest and northernmost ice caps (Northern Ellesmere and Agassiz) have large accumulation areas and relatively small ablation areas. On these ice caps either the percolation (Agassiz) or saturation (Northern Ellesmere) zones are the most extensive facies. The smallest ice caps (Sydkap, Manson, and Axel Heiberg) have large ablation areas and the superimposed and glacier ice zones are the most extensive facies (Table 3).

4.3. Interannual Variability in Facies Distribution

[19] Standard deviations of facies areas, normalized by the area of each facies, indicate that the glacier ice zone has the most variable area on all ice caps in the QEI combined, followed by the percolation, saturation, and superimposed ice zones (Table 4). For individual ice caps, however, the relative variability in the areas of the different facies differs considerably. On Agassiz, Northern Ellesmere, and POW the glacier ice zone has the most variable facies area followed by the percolation, superimposed ice, and saturation zones, whereas, on Axel Heiberg, Devon, Manson, and Sydkap the percolation zone area has the greatest variability, followed by the glacier ice, saturation, and superimposed ice zones. The areas of the percolation and saturation zones are most variable on Sydkap and least variable on Agassiz and Northern Ellesmere, respectively. Variability in the areas of the superimposed and glacier ice zones is greatest on POW and Agassiz, respectively, and least on Devon. Combined normalized standard deviations of snow and ice surface facies areas indicate that the greatest overall variability occurs on Sydkap, while the least variability for all facies combined occurs on the Devon ice cap.

[20] Standardized annual anomalies of the snow and ice facies areas on the QEI ice caps for the 7-year period are shown in Figure 6. There is significant interannual variability for the QEI as a whole, and changes in the areas of the percolation and saturation zones are negatively correlated with changes in those of the superimposed and glacier ice facies. For all ice caps in the QEI combined, positive anomalies in the percolation zone area occurred in all years except 2001 and 2003. Positive anomalies in percolation zone area occurred on all ice caps in 2002, 2004, and 2005, except on Manson (2002 and 2005) where negative facies area anomalies occurred. There was a mix of positive and negative anomalies in 1999 and 2000. Strong negative anomalies in percolation zone area occurred on all ice caps in 2001 and, in 2003, negative anomalies occurred on all ice caps except Agassiz and Northern Ellesmere. Positive standardized anomalies in the saturation zone area occurred on nearly all QEI ice caps in all years except 2001, when strongly negative anomalies in the area of this facies occurred on all ice caps. Anomalies in the area of the superimposed ice zone are variable throughout the 1999–2005 period, but are essentially the opposite of anomalies in the area of the percolation zone, with negative values in 2004 and mostly negative values in 2002 and 2005. Mainly positive anomalies occurred in 2001 and 2003. Standardized

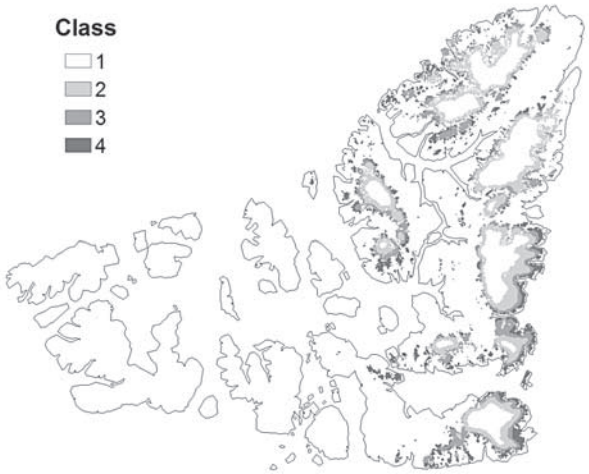

Figure 3. Results of the ISODATA classification of the average 1999–2005 postfreeze-up biweekly-average σ^0 image (Figure 2a).

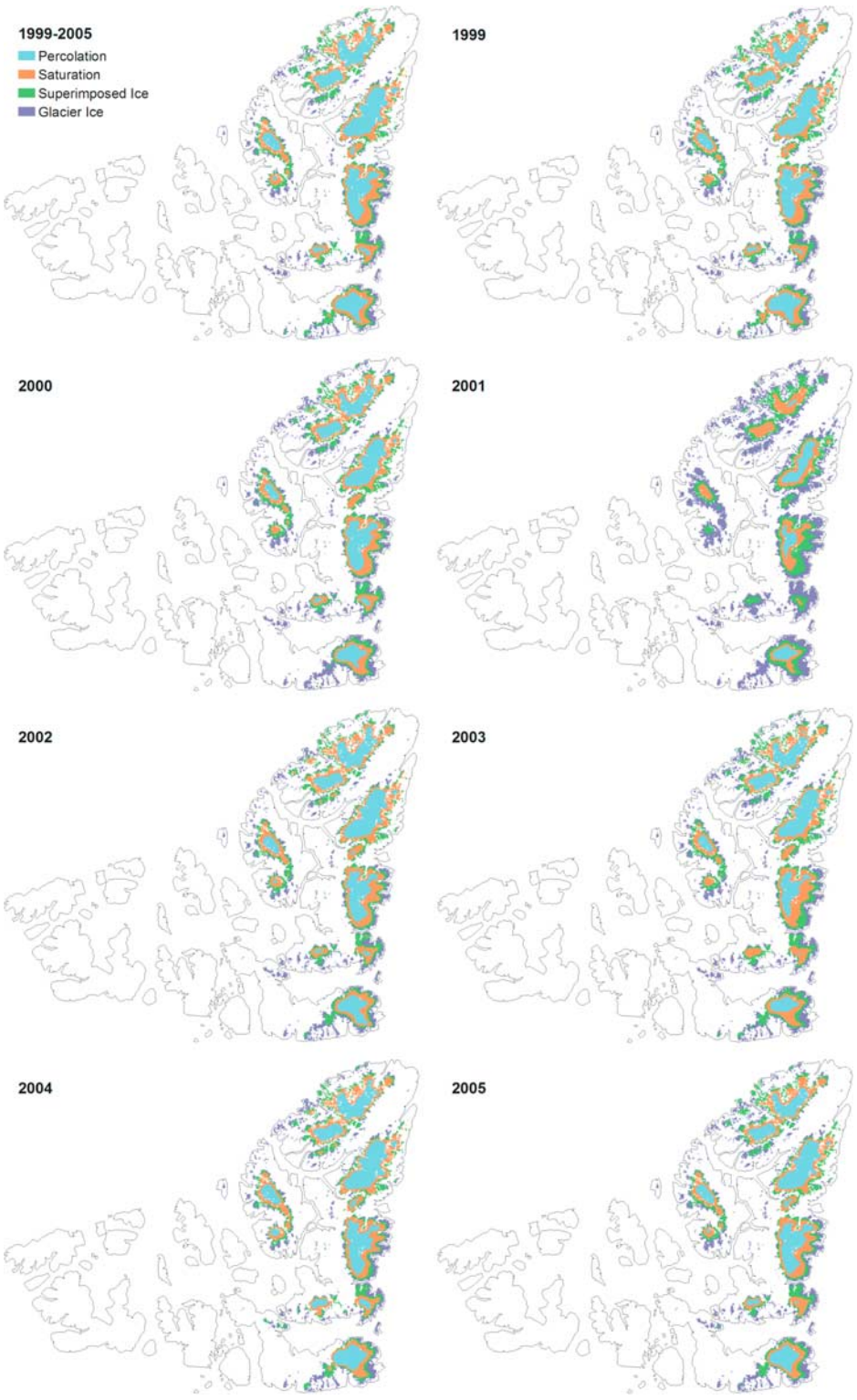

Figure 4. Maps of snow and ice surface facies distribution on ice caps in the QEI, 1999–2005. Annual facies maps are the result of supervised classification of backscatter signatures derived from the ISODATA classification (Figure 3).

anomalies of glacier ice area are negative for all years except 2000 when slightly positive anomalies occurred on Devon and 2001 when strong positive anomalies occurred on all ice caps.

4.4. Facies Variability and Climatic Controls

[21] Clear relationships between QS derived melt duration and summer-averaged (JJA) geopotential height (between 700 and 300 hPa) were discovered in previous

Table 2. Facies Classification Statistics Resulting From ISODATA Classification of QS Postfreeze-Up Biweekly-Averaged σ^0 (1999–2005) On Ice Caps in the QEI[a]

Year	Facies	Minimum	Maximum	Mean	Standard Deviation
1999	Percolation	−3.45	−1.50	−2.72	0.45
	Saturation	−5.08	−3.46	−4.26	0.48
	Superimposed	−6.51	−5.09	−5.80	0.41
	Glacier Ice	−14.06	−6.52	−7.77	1.13
2000	Percolation	−3.71	−1.92	−2.97	0.44
	Saturation	−5.35	−3.72	−4.53	0.48
	Superimposed	−6.75	−5.36	−6.06	0.40
	Glacier Ice	−13.13	−6.76	−7.87	0.97
2001	Percolation	−2.48	−1.46	−2.13	0.24
	Saturation	−3.62	−2.49	−3.07	0.33
	Superimposed	−5.15	−3.63	−4.38	0.44
	Glacier Ice	−14.54	−5.16	−6.70	1.14
2002	Percolation	−4.21	−2.23	−3.49	0.43
	Saturation	−5.67	−4.22	−4.93	0.43
	Superimposed	−6.90	−5.68	−6.26	0.35
	Glacier Ice	−13.61	−6.91	−7.94	0.91
2003	Percolation	−3.79	−1.97	−3.02	0.45
	Saturation	−5.39	−3.80	−4.63	0.45
	Superimposed	−6.75	−5.40	−6.05	0.39
	Glacier Ice	−14.22	−6.76	−7.90	1.00
2004	Percolation	−4.18	−2.47	−3.51	0.40
	Saturation	−5.57	−4.19	−4.88	0.40
	Superimposed	−6.75	−5.58	−6.12	0.34
	Glacier Ice	−14.47	−6.76	−7.80	0.96
2005	Percolation	−3.40	−1.83	−2.73	0.37
	Saturation	−4.97	−3.41	−4.16	0.45
	Superimposed	−6.41	−4.98	−5.68	0.41
	Glacier Ice	−13.93	−6.42	−7.65	1.10

[a]QS postfreeze-up biweekly-averaged σ^0 from the period 1999–2005.

work on ice caps in Arctic Canada and on the Greenland Ice Sheet [*Wang et al.*, 2005, 2007]. In this study, we investigated the relationships between facies area and boundary elevation changes on the QEI ice caps and geopotential height and air temperature in the troposphere at a point above the approximate center of each ice cap (Figure 7 and Table 5). For the QEI as a whole, correlation analysis indicates that changes in the troposphere (700, 500, and

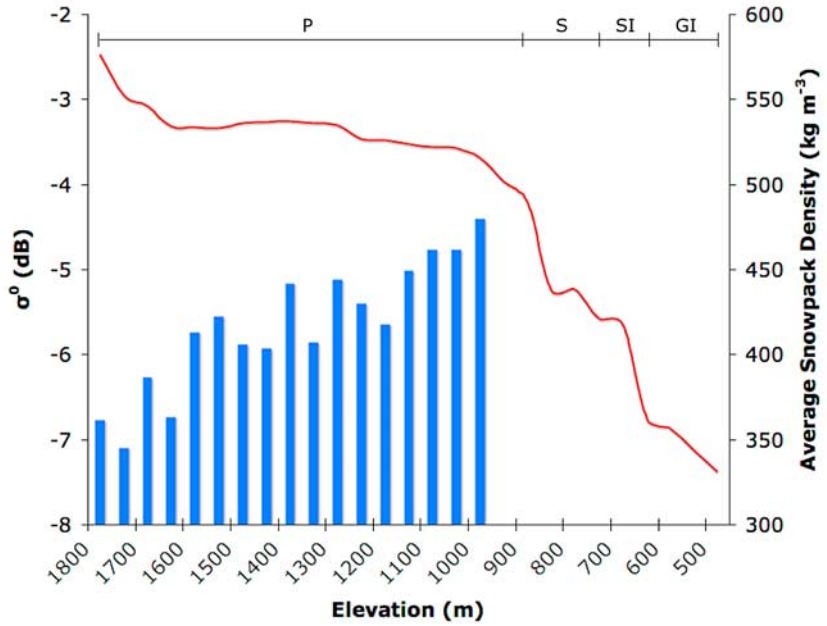

Figure 5. Postfreeze-up biweekly-average σ^0 (line) and autumn average snowpack density (from *Bell et al.* [2008]) for each 50-m elevation band along the Cryosat Transect, Devon Ice Cap, in 2004. Approximate boundaries for percolation (P), saturation (S), superimposed ice (SI), and glacier ice (GI) zones, determined from ISODATA classification, are indicated.

Table 3. Area of Each Facies Expressed as a Percentage of the Total Ice Cap Area for Each Ice Cap in the QEI for the Period 1999–2005[a]

Ice Cap	Total Area	Facies	1999	2000	2001	2002	2003	2004	2005	Mean	Standard Deviation
QEI	113,418.8	Percolation	27.2	25.9	7.9	29.5	22.5	32.9	28.2	23.7	9.7
	113,418.8	Saturation	28.0	26.9	16.9	29.5	28.4	28.1	26.7	26.0	5.1
	113,418.8	Superimposed	23.5	23.2	25.6	22.2	26.4	20.6	23.3	23.6	2.4
	113,418.8	Glacier Ice	21.4	23.9	49.6	18.8	22.7	18.4	21.8	26.7	13.0
Devon	16,035.1	Percolation	30.7	21.8	13.0	28.1	17.2	31.5	27.2	22.3	7.6
	16,035.1	Saturation	26.7	22.6	13.4	23.2	24.3	23.2	21.4	21.3	4.5
	16,035.1	Superimposed	19.9	17.4	22.6	20.1	26.4	20.2	21.9	21.3	3.4
	16,035.1	Glacier Ice	22.8	38.3	51.1	28.6	32.0	25.2	29.5	35.0	10.2
Sydkap	3747.6	Percolation	11.1	8.1	0.0	7.3	0.0	26.7	15.5	8.4	10.9
	3747.6	Saturation	25.5	23.2	0.5	24.0	30.8	33.8	23.9	22.5	13.1
	3747.6	Superimposed	30.3	31.0	23.4	32.9	42.3	24.7	28.5	30.9	7.6
	3747.6	Glacier Ice	33.2	37.6	76.1	35.8	26.9	14.8	32.1	38.3	23.0
Manson	6232.8	Percolation	3.5	7.5	0.0	4.1	0.7	11.3	1.4	4.7	4.7
	6232.8	Saturation	23.7	24.6	3.1	25.7	29.4	28.4	29.5	22.3	10.9
	6232.8	Superimposed	35.0	39.9	22.0	40.0	40.6	33.7	38.9	35.2	7.9
	6232.8	Glacier Ice	37.8	28.0	74.9	30.1	29.3	26.6	30.2	37.8	20.8
POW	20,703.5	Percolation	36.2	38.5	10.5	36.4	24.1	38.3	38.2	29.6	12.2
	20,703.5	Saturation	33.4	32.5	24.0	35.1	38.0	32.1	33.3	32.3	5.2
	20,703.5	Superimposed	15.4	16.0	34.2	17.3	22.8	15.4	16.2	21.1	7.9
	20,703.5	Glacier Ice	15.1	13.0	31.3	11.3	15.1	14.2	12.3	17.0	8.1
Agassiz	21,465.9	Percolation	41.1	39.6	20.7	46.2	40.0	49.6	45.5	39.2	11.2
	21,465.9	Saturation	31.2	31.0	21.8	33.2	31.1	29.0	28.5	29.2	4.4
	21,465.9	Superimposed	21.6	22.9	26.5	15.6	22.3	15.8	20.2	20.6	4.8
	21,465.9	Glacier Ice	6.2	6.4	31.0	5.0	6.6	5.6	5.9	10.9	11.2
N Ellesmere	24,371.9	Percolation	30.4	30.3	1.2	37.8	32.0	38.1	30.2	27.9	15.3
	24,371.9	Saturation	32.7	32.4	24.6	34.3	30.5	31.7	31.1	30.7	3.7
	24,371.9	Superimposed	26.2	25.2	32.4	21.7	24.9	22.0	25.8	25.3	4.3
	24,371.9	Glacier Ice	10.7	12.1	41.8	6.3	12.6	8.2	13.0	16.2	14.6
Axel Heiberg	11,916.2	Percolation	13.2	10.6	0.0	14.6	11.0	22.5	16.4	11.7	8.1
	11,916.2	Saturation	27.4	26.4	9.8	32.9	27.5	35.7	29.5	26.4	10.0
	11,916.2	Superimposed	32.9	33.4	19.5	32.1	35.1	25.0	30.3	29.0	6.6
	11,916.2	Glacier Ice	26.5	29.7	70.7	20.4	26.4	16.8	23.8	32.8	21.7

[a]Total ice cap area given in km^2. Mean and standard deviation values were computed for the 7-year period.

300 hPa geopotential heights) are negatively correlated with changes in the areas of percolation and saturation facies, and positively correlated with area changes in the superimposed and glacier ice facies (Table 5). Facies area changes are most strongly correlated with geopotential height in the middle to upper troposphere, and the correlations are statistically significant ($p < 0.01$; except for the superimposed ice zone). JJA air temperature at the 700 hPa level is significantly ($p < 0.01$) and positively correlated ($r = 0.40$) with the glacier ice zone area and negatively correlated with the areas of the saturation and percolation facies ($r = -0.40$ and -0.34 ($p < 0.05$), respectively). In addition, summer geopotential height in the troposphere and temperatures at the 700 hPa level over ice caps in the QEI are positively correlated with changes in facies boundary elevations. For instance, 700 hPa JJA air temperature over the Devon Island ice cap is positively correlated with the saturation and snow/firn line elevations ($r = 0.40$ and 0.50, respectively ($p < 0.05$)) along the Cryosat transect. These findings indicate that increases in air temperature are coincident with increases in the area of the superimposed and glacier ice zones, and with a decrease in the area of percolation and saturation zone facies and an upward shift in facies boundary elevations.

4.5. Autumn σ^0 and Melt Duration

[22] Melt duration derived from near-surface air temperature measurements is well correlated with melt duration estimates derived from QS and provides a means of characterizing melt conditions on Arctic ice caps [*Wang et al.*, 2005, 2007]. To investigate the influence of melt duration on autumn σ^0, and thereby its influence on changes in facies distribution, we regressed annual QS postfreeze-up biweekly-averaged σ^0 against annual QS melt duration for each pixel for the period 2000–2005 (Figure 8). There are significant spatial variations in both the strength and sign of the regression coefficient across the QEI ice caps. In general, r values are positive at high elevations, negative to strongly negative at low elevations, and variable at intermediate elevations..

Table 4. Standard Deviations of Facies Areas, Normalized by the Area of Each Facies, on All Ice Caps in the QEI for the Period 1999–2005

Facies	QEI	Devon	Sydkap	Manson	POW	Agassiz	N Ellesmere	A Heiberg
Percolation	0.41	0.34	1.30	1.00	0.41	0.28	0.55	0.69
Saturation	0.20	0.21	0.58	0.49	0.16	0.15	0.12	0.38
Superimposed	0.10	0.16	0.24	0.22	0.37	0.23	0.17	0.23
Glacier Ice	0.49	0.29	0.60	0.55	0.48	1.03	0.90	0.66

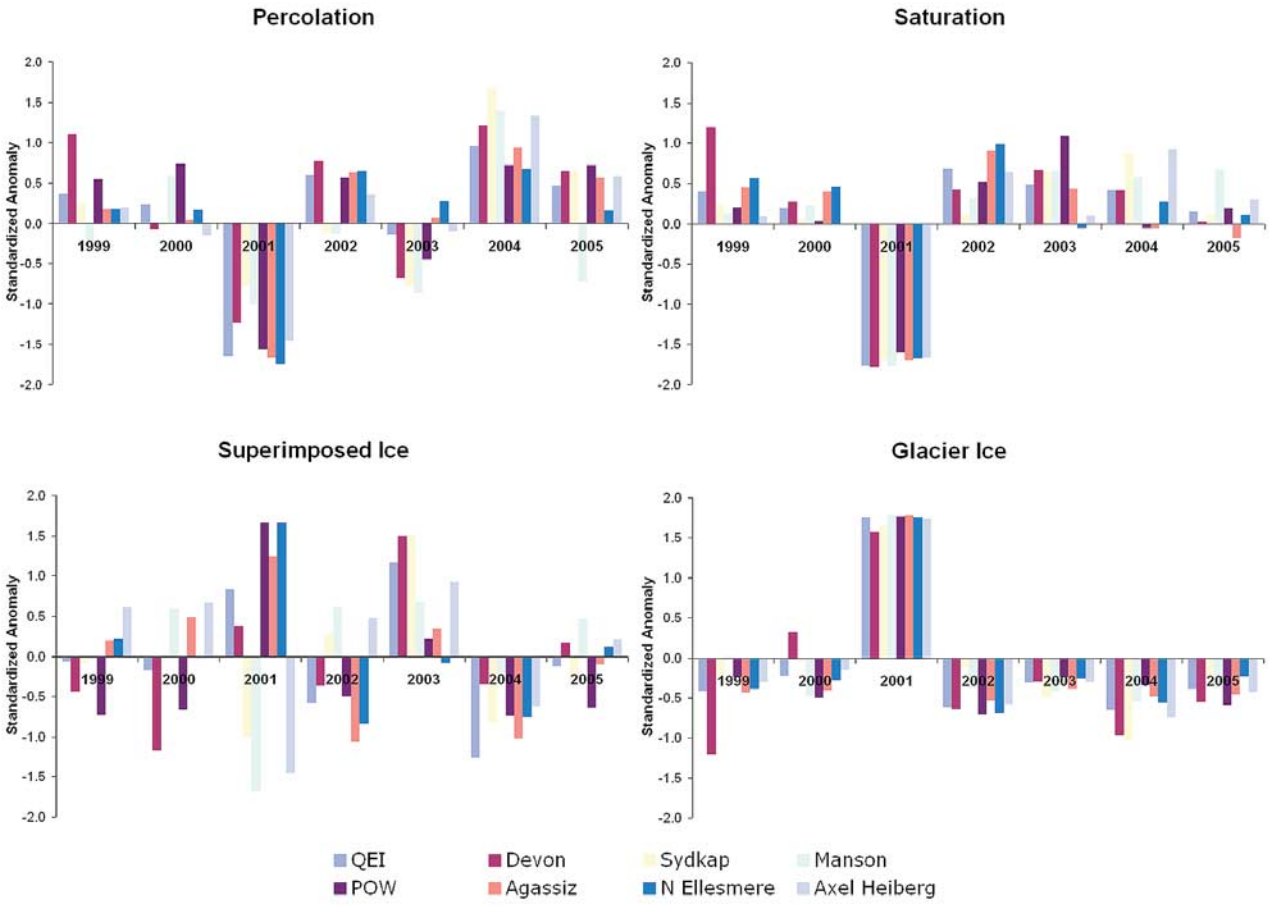

Figure 6. Standardized anomalies of snow and ice surface facies area for ice caps in the QEI, 1999–2005. Anomalies are expressed with respect to the 2000–2004 climatology period for consistency with previous studies [*Wang et al.*, 2005, 2007; *Sharp and Wang*, 2009].

[23] The northern ice caps (N Ellesmere, Agassiz, and Axel Heiberg) show increasing autumn backscatter with increasing melt duration at high elevations, and decreasing autumn backscatter with increasing melt duration at low elevations. Agassiz and Axel Heiberg show a positive relationship between melt duration and autumn σ^0 in the percolation zone and either negative or no relationships in other facies zones. However, N Ellesmere shows strongly positive r values in the upper percolation zone but decreasing r values with decreasing elevation through the lower percolation zone and other facies zones.

[24] Ice caps/fields in the southeast QEI (Devon, POW, Manson, and Sydkap) show a similar overall distribution of the regression coefficient as the northern ice caps, but the spatial patterns are more complicated. POW shows mostly positive r values in the high-elevation areas in the north-

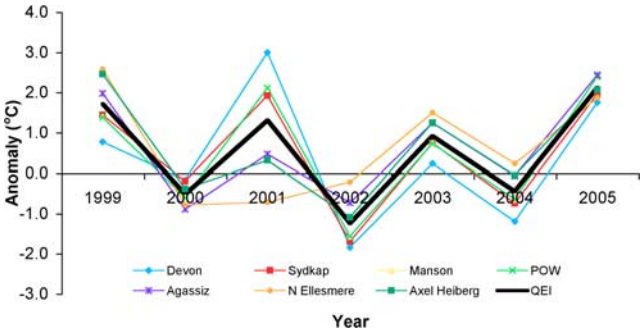

Figure 7. July air temperature at the 700 hPa level over each ice cap in the QEI, 1999–2005. Anomalies are expressed with respect to the 2000–2004 climatology period for consistency with previous studies [*Wang et al.*, 2005, 2007; *Sharp and Wang*, 2009].

Table 5. Correlation Coefficients Between Facies Area on All Ice Caps in the QEI and Summer-Averaged Geopotential Height at the 500 and 300 hPa Levels and Air Temperature at the 700 hPa Level Above Each Ice Cap

Facies	Geopotential Height		Air Temperature at 700 hPa
	500 hPa	300 hPa	
Percolation	−0.44	−0.45	−0.34
Saturation	−0.53	−0.47	−0.40
Superimposed[a]	0.08	0.13	0.04
Glacier Ice	0.52	0.47	0.40

[a]Correlations are statistically significant ($p < 0.01$) except for the superimposed ice zone.

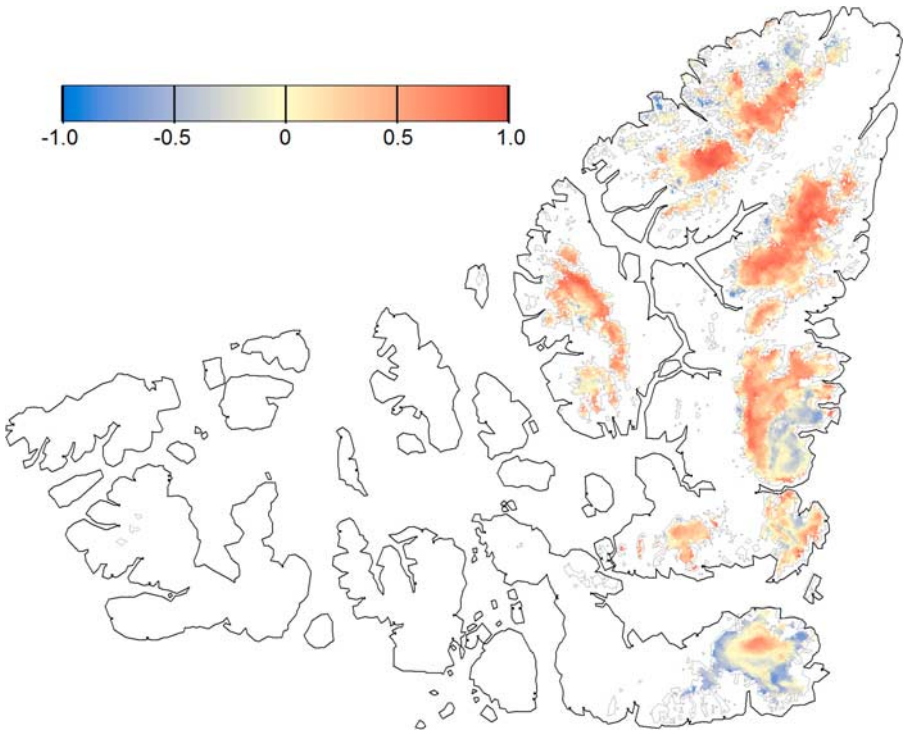

Figure 8. QS postfreeze-up biweekly-averaged σ^0 regressed upon melt duration at each pixel for the 2000–2005 pentad.

west, and mostly negative values at low elevations in the west and the southeast. The boundary between the two patterns found on POW lies along the topographic high created by the NE–SW trending Prince of Wales Mountains that divide the icefield. Manson shows a similar contrast in the spatial pattern of r values brought about largely by the influence of mountains crossing the icefield. Sydkap shows positive r values at high elevations and on the south arm of the ice cap. Negative r values are found mostly at low elevations along the west and northwest margin of the ice cap. On the Devon Ice Cap, regression coefficients are strongly positive at the summit and strongly negative at low elevations near the margins of the ice cap. Intermediate elevations mostly show positive regression coefficients, but there are some areas on the southern part of the ice cap where the r values are slightly negative.

[25] An increase in melt duration in the upper percolation zone generally leads to an increase in the percolation and refreezing of meltwater and the formation of stratigraphic discontinuities at depth in the snowpack, which leads to an increase in autumn σ^0. As melt duration within the percolation zone decreases, so do the production of refrozen melt features in the snowpack and the autumn σ^0 signal. However, some regions of the percolation zone on QEI ice caps exhibit a decrease in autumn σ^0 as melt duration increases (e.g., Devon and POW). For instance, the southeast percolation zone on POW shows a sizable region of negative regression coefficients (Figure 8). This region typically experiences one of the longest melt seasons and has one of the highest snow accumulation rates in the QEI [*Wang et al.*, 2005; *Koerner*, 2002]. Weeks of positive air temperatures produce large amounts of meltwater, which percolate into the snow and firn. In years with particularly long or intensely warm melt seasons, at the autumn freeze-up there could be a significant amount of meltwater that remains (unfrozen) in the snowpack beneath the frozen surface, which could reduce the backscatter from deeper frozen layers, thereby reducing the volume scattering contribution to the backscatter signal. This effect could be exacerbated if the end of summer is marked by heavy snowfall rather than freezing of the surface, which is very likely, given that this region receives the highest snowfall in the QEI [*Koerner*, 1979], much of which accumulates in autumn (e.g., 2000 and 2004, Figure 9).

4.6. Ice Layer Formation: Signature and Detection

[26] Interannual changes in QS postfreeze-up biweekly-averaged σ^0 have been used in previous studies to map regions of ice layer formation on the Greenland Ice Sheet [*Nghiem et al.*, 2005; *Wang et al.*, 2007]. Both *Nghiem et al.* [2005] and *Wang et al.* [2007] identified abrupt changes in the QS σ^0 response after melt periods in the percolation zone on the Greenland Ice Sheet. Ice layers (i.e., ice features and layers) form in the snowpack when meltwater percolates into the snowpack and refreezes. Ice layers can include coalesced ice granules and ice pipes, layers, and lenses, all of which are effective Ku-band scatterers. Ice layer formation causes an increase in σ^0 at the end of each melt season, while an increase in σ^0 between the periods immediately following successive melt seasons implies a greater degree of ice layer formation in the second melt season. On the basis of field observations, Nghiem *et al.*, confirmed that the postmelt period σ^0 jump (2002) was due to the formation of a 2 cm thick ice layer and other percolation features in the snowpack. Decreases in σ^0 between successive melt seasons would imply reduced ice layer formation in the second summer.

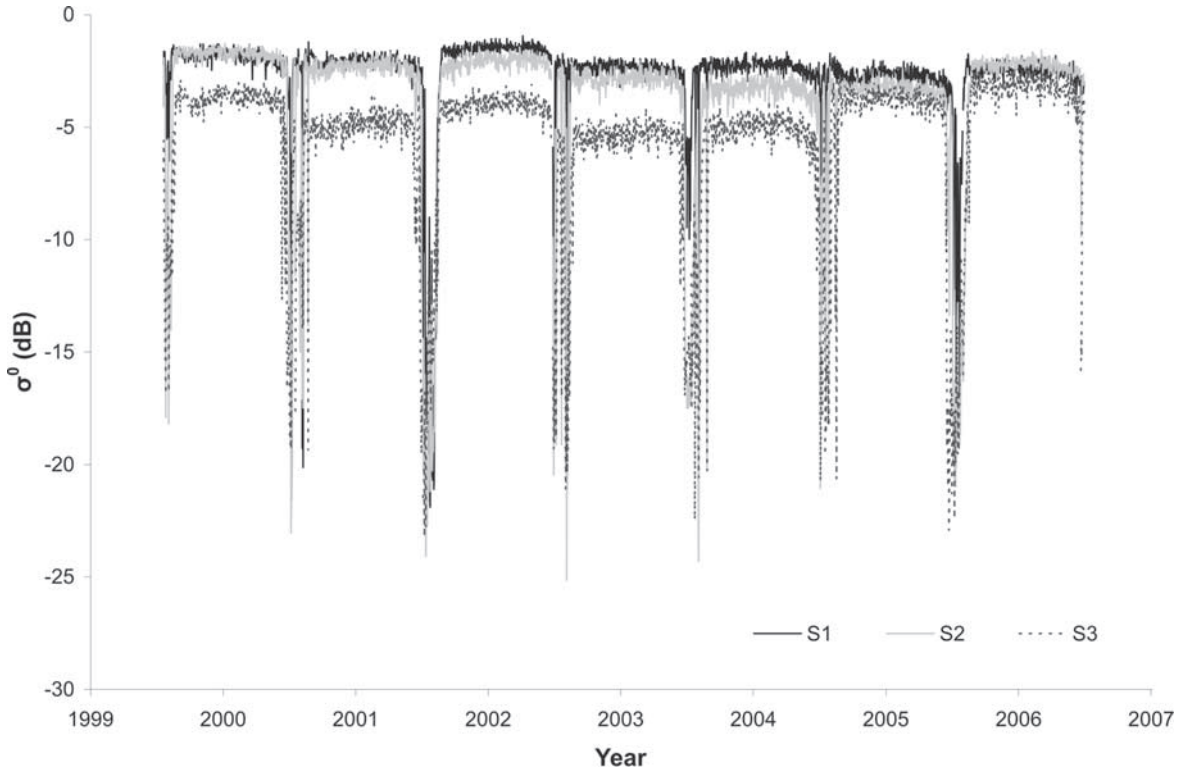

Figure 9. Time series of QS backscatter response at sites S1, S2, and S3 on the Cryosat Transect, Devon Ice Cap, 1999–2006.

[27] We observe similar behavior in the σ^0 signal from sites in the percolation zone of QEI ice caps. Figure 9 shows the backscatter response for the period 1999–2005 for three sites along the Cryosat transect on Devon (Figure 1). Sites S1 (1802 m) and S2 (1415 m) are always in the percolation zone, while site S3 (994 m) is near the mean position of the snow/firn line (i.e., the boundary between the saturation zone and superimposed ice zone) and is in all facies zones, except the glacier ice zone, intermittently during the period of record. Following the 2001 melt season, only a slight change in σ^0 was detected at S2, but there was an obvious increase in σ^0 at S1 and S3 (0.30 and 0.80 dB, respectively) compared to the previous postmelt season period (2000), indicating that new or more extensive ice layers had formed in the snowpack. Conversely, following the 2002 melt season, a σ^0 decrease was experienced at all three sites (S1 = −0.72, S2 = −0.57, S3 = −1.06 dB), suggesting a reduction in the abundance of new ice layers relative to the preceding melt season, or the accumulation of new snow on the surface during or prior to the autumn freeze-up.

[28] Algorithms for the detection of ice layer formation on the Greenland Ice Sheet were first developed by *Nghiem et al.* [2005] and refined by *Wang et al.* [2007]. Nghiem *et al.*, calculated the biweekly-averaged σ^0 change between fixed periods before and after the same melt season for the entire ice sheet. To avoid biases inherent to this approach, Wang *et al.*, used the change in QS postfreeze biweekly-averaged σ^0 between successive years to identify ice layer formation. They calculated the change in biweekly-averaged σ^0 for each pixel, beginning two weeks after the end of successive melt seasons, as indicated by the freeze-up date determined for each pixel in each year. The current study uses the approach developed by Wang *et al.*, to detect ice layer formation in the percolation and dry snow zones for each pixel and map its distribution on QEI ice caps for the period 2000–2005.

4.7. Ice Layer Formation: Spatial Distribution and Interannual Changes, 2000–2005

[29] Figure 10 shows maps of the postfreeze biweekly-averaged σ^0 change between successive melt seasons for QEI ice caps in the years 2000–2005. Yellow to red colors represent positive σ^0 values, and in the percolation zone, this indicates that there was an increase in σ^0 resulting from a more significant fraction of ice layers in the near surface snow/firn in that region since the end of the previous melt season. Higher values of σ^0 change (dark red) imply either that ice layers became much more significant in this area or that the snowpack became more complex (i.e., more inhomogeneities). Light blue to dark blue colors represent negative σ^0 values, indicating a decrease in σ^0 in these regions since the previous autumn, which suggests that new ice layer formation was either limited or nonexistent, or that there was considerable snowfall at the end of the melt season.

[30] Overall, ice layer formation in the percolation zone was highly variable during the 6-year period (2000–2005) on the QEI ice caps. The most extensive ice layer formation occurred in 2005 and 2001, when there were strongly positive air temperature anomalies at the 700 hPa level (Figure 7). In 2005, ice layers formed on all ice caps and large values of σ^0 change were ubiquitous, with the greatest σ^0 changes found on POW. In 2001, both POW and Devon had large σ^0 change values, but no ice layer formation was

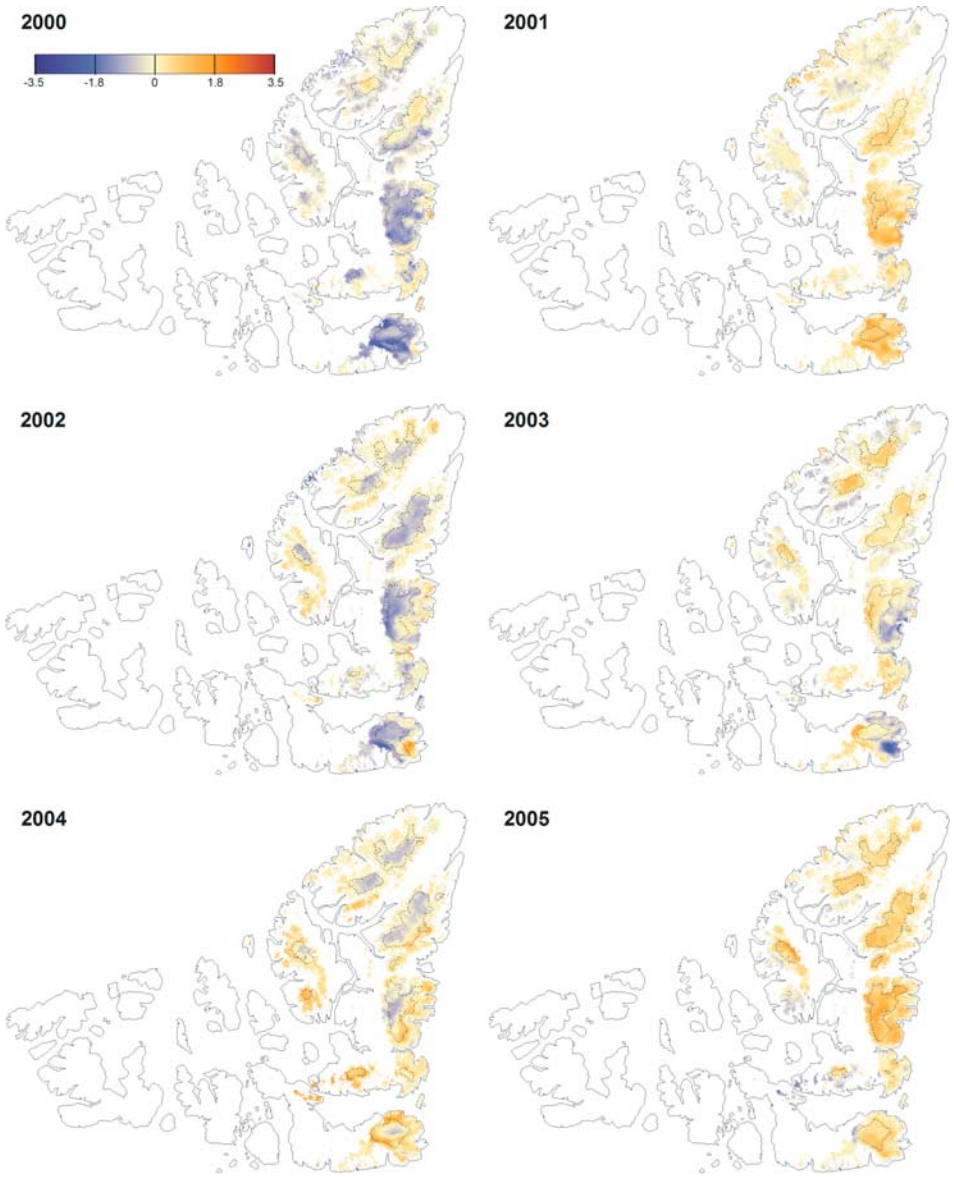

Figure 10. Maps of the postfreeze-up biweekly-averaged σ^0 change between successive melt seasons for ice caps in the QEI for the years 2000–2005. The dashed line marks the position of the saturation line for each year, which delimits the lower extent of the percolation zone. In the percolation zone, positive values (yellow to red) represent areas of more significant ice layer formation since the previous summer; whereas negative values (blue) indicate areas where new ice layer formation since the previous melt season was limited or nonexistent.

detected at high elevations in N Ellesmere, Axel Heiberg or Sydkap. 2000 and 2002 had the least extensive ice layer formation, but their spatial patterns of ice layer formation were very different. In 2000, ice layer formation was very limited on Devon, Sydkap, Manson, POW, and Axel Heiberg and occurred only at high elevations on Agassiz and N Ellesmere. In 2002, ice layer formation generally occurred on the lowest areas of the percolation zone, whereas, high-elevation areas had strongly negative σ^0 changes. For ice caps in the southeast QEI (POW, Manson, and Devon) ice layer formation only occurred on the east side of these percolation zones. The 2003 spatial pattern of σ^0 change and therefore, ice layer formation, is essentially the reverse of the 2002 pattern. In 2002 and 2004, large decreases in σ^0 occurred above the melt limit on N Ellesmere and Agassiz.

[31] The distribution and magnitude of ice layer formation can be affected by melt period length and late season snowfall. Widespread or localized ice layer formation can occur on QEI ice caps after only a few days of melt, which is consistent with findings on the Greenland Ice Sheet [*Wang et al.*, 2007]. Heavy snowfall at the end of the melt season could affect the apparent spatial distribution of ice layer formation (Figure 10) either by precluding the formation of a distinct ice layer or significantly attenuating the backscatter signal. Because snow accumulation is very low in most of the QEI, this effect is believed to be limited to the highest-snowfall areas in the southeast (i.e., near Baffin

Bay), and it is likely to have played a role in the apparent distribution of ice layer formation in both 2000 and 2004.

[32] Interannual variations in the distribution and magnitude of ice layer formation in the percolation zone can have a significant influence on variations in near surface firn density. Density variations in the near surface firn can lead to difficulty in interpreting elevation change measurements derived from radar and laser altimeters in terms of changes in glacier mass balance. In addition, changes in the vertical distribution of strong reflectors in the snowpack relative to the surface, due to either snow accumulation (e.g., 2000 and 2004) or interannual variability in the spatial distribution of ice layer formation, may result in errors in the measurement of surface elevation (and hence elevation change) by radar altimetry.

5. Summary and Conclusions

[33] This study serves as a useful validation of enhanced resolution scatterometer data. Enhanced resolution slice data from the SeaWinds scatterometer on board QS were used to map the distribution of snow and ice facies and its interannual variability during the period 1999–2005. ISODATA classification of the average postfreeze-up biweekly-average σ^0 signal for the 7-year period resulted in the delineation of percolation, saturation, superimposed ice, and glacier ice facies on ice caps in the QEI. The glacier ice zone is the most extensive facies in the QEI and represents 26.7% of the total ice covered area, followed by the saturation, percolation, and superimposed ice zones (26.0, 23.7, and 23.6%, respectively). Although an intermittent dry snow zone exists on some of these ice caps and can be identified using maps of QS derived melt extent, it is not detectable using the postfreeze biweekly-average σ^0 signal, because of the low annual snow accumulation and microwave interaction with buried melt features in the firn layer.

[34] Interannual variability in the area of snow and ice facies and the elevations of the boundaries between facies were investigated. For the QEI as a whole, variability in facies area is greatest for the glacier ice zone and least for the superimposed ice zone. Area changes in the superimposed and glacier ice zones are negatively correlated with changes in the percolation and saturation zones. Changes in JJA geopotential height in the troposphere (700, 500, and 300 hPa) and JJA air temperature at the 700 hPa level are positively (negatively) correlated with changes in the glacier ice zone (percolation and saturation zones) area and with elevation changes in facies boundary elevations. In addition, melt duration and postfreeze biweekly-average backscatter exhibit positive (negative) correlations at high (low) elevation. These results indicate that increases in air temperature and melt duration are generally associated with an increase in the area of the glacier ice zone, a decrease in the area of percolation and saturation zones, and an increase in the elevation of interfacies boundaries.

[35] The change in biweekly-averaged backscatter of each pixel following the freeze-up periods in successive autumns was used to map changes in the distribution of ice layers formed by meltwater percolation and refreezing in the snow and firn within the percolation zone. Results indicate a high degree of spatiotemporal variability in ice layer formation in the percolation zone on QEI ice caps. Heavy snowfall at the end of the 2000 and 2004 melt seasons may be a source of error in the apparent spatial distribution of ice layer formation. The most extensive ice layer formation occurred in 2001 and 2005, with 2005 showing large magnitude backscatter changes over the previous year's values at nearly all locations in the percolation zones of all ice caps. During the 6-year period, ice layers formed in some regions in only a few days, which is consistent with observations on the Greenland Ice Sheet by *Wang et al.* [2007]. This suggests that simply reaching the melting point may be sufficient to form a spatially extensive ice layer. Areas experiencing large magnitude positive backscatter change from the previous year are likely to be associated with the greatest changes in the density profile of the snowpack, and therefore changes in the surface height, which could signify those areas where errors are most likely to occur when estimating mass balance from surface elevation change measurements from satellite or airborne altimeters. Maps of the interannual changes in the distribution of ice layers resulting from this study will be valuable for quality control and the interpretation of radar altimetric measurements of surface elevation change and as a proxy indicator of climate variability across the Arctic ice caps.

[36] The results from this study underscore the importance of understanding the complex and dynamic linkages between climatic forcings, changes in the troposphere, and ice cap surface responses. We present here, an efficient means of monitoring the interannual variability in snow and ice surface properties resulting from changes in melt conditions on ice caps in the Canadian High Arctic. Surface melt is an important component of the surface mass balance, and changes in seasonal melt extent can be a good indicator of climatic change [*Bindschadler*, 1998]. Mapping annual facies distributions on Arctic ice caps will provide a more detailed view of seasonal melt conditions than maps of melt extent alone, and may be useful for estimating the surface mass balance of ice caps in remote polar regions.

[37] **Acknowledgments.** This work was supported by the Canadian Foundation for Climate and Atmospheric Sciences through the Polar Climate Stability Network, Environment Canada, through the CRYSYS program and NSERC Canada (through a Discovery Grant awarded to M. Sharp). We thank David Long for assistance with obtaining the QuikSCAT data and Christina Bell and David Burgess for providing snowpack data. We acknowledge helpful reviews by three anonymous referees.

References

Abdalati, W., W. Krabill, E. Frederick, S. Manizade, C. Martin, J. Sonntag, R. Swift, R. Thomas, J. Yungel, and R. Koerner (2004), Elevation changes of ice caps in the Canadian Arctic Archipelago, *J. Geophys. Res.*, *109*, F04007, doi:10.1029/2003JF000045.

Bardel, P., A. G. Fountain, D. K. Hall, and R. Kwok (2002), Synthetic aperture radar detection of the snowline on Commonwealth and Howard glaciers, Taylor Valley, Antarctica, *Ann. Glaciol.*, *34*, 177–183, doi:10.3189/172756402781818021.

Bell, C., D. Mair, D. Burgess, M. Sharp, M. Demuth, F. Cawkwell, R. Bingham, and J. Wadham (2008), Spatial and temporal variability in the snowpack of a High Arctic Ice Cap: Implications for mass-change measurements, *Ann. Glaciol.*, *48*, 159–170, doi:10.3189/172756408784700725.

Benson, C. S. (1962), Stratigraphic studies in the snow and firn of the Greenland Ice Sheet, *Res. Rep. 70*, 120 pp., Cold Reg. Res. and Eng. Lab., Hanover, N. H.

Bindschadler, R. (1998), Monitoring ice sheet behavior from space, *Rev. Geophys.*, *36*, 79–104, doi:10.1029/97RG02669.

Bindschadler, R., and P. Vornberger (1992), Interpretation of SAR imagery of the Greenland Ice-Sheet using coregistered TM imagery, *Remote Sens. Environ.*, *42*, 167–175, doi:10.1016/0034-4257(92)90100-X.

Bindschadler, R., J. Dowdeswell, D. Hall, and J. G. Winther (2001), Glaciological applications with Landsat-7 imagery: Early assessments, *Remote Sens. Environ.*, *78*, 163–179, doi:10.1016/S0034-4257(01)00257-7.

Braithwaite, R. J., M. Laternser, and W. T. Pfeffer (1994), Variations of near-surface firn density in the lower accumulation area of the Greenland Ice Sheet, Pakitsoq, west Greenland, *J. Glaciol.*, *40*, 477–485.

Braun, M., F. Rau, H. Saurer, and H. Gossmann (2000), Development of radar glacier zones on the King George Island ice cap, Antarctica, during austral summer 1996/97 as observed in ERS-2 SAR data, *Ann. Glaciol.*, *31*, 357–363, doi:10.3189/172756400781819950.

Davis, C. H., C. A. Kluever, and B. J. Haines (1998), Elevation change of the southern Greenland Ice Sheet, *Science*, *279*, 2086–2088, doi:10.1126/science.279.5359.2086.

Dyurgerov, M., and M. Meier (2005), Glaciers and the changing earth system: A 2004 snapshot, *Occas. Pap. 58*, 118 pp., Inst. of Arctic and Alp. Res., Boulder, Colo.

Engeset, R. V., J. Kohler, K. Melvold, and B. Lundén (2002), Change detection and monitoring of glacier mass balance and facies using ERS SAR winter images over Svalbard, *Int. J. Remote Sens.*, *23*, 2023–2050, doi:10.1080/01431160110075550.

Fahnestock, M., R. Bindschadler, R. Kwok, and K. Jezek (1993), Greenland Ice Sheet surface-properties and ice dynamics from ERS-1 SAR imagery, *Science*, *262*, 1530–1534, doi:10.1126/science.262.5139.1530.

Gardner, A. S., and M. Sharp (2009), Sensitivity of net mass balance estimates to near-surface temperature lapse rates when employing the degree day method to estimate glacier melt, *Ann. Glaciol.*, *50*, 80–86.

Greuell, W., and W. H. Knap (2000), Remote sensing of the albedo and detection of the slush line on the Greenland Ice Sheet, *J. Geophys. Res.*, *105*, 15,567–15,576, doi:10.1029/1999JD901162.

Hall, D. K., J. P. Ormsby, R. A. Bindschadler, and H. Siddalingaiah (1987), Characterization of snow and ice reflectance zones on glaciers using Landsat thematic mapper data, *Ann. Glaciol.*, *9*, 104–108.

Hassol, S. J. (2004), *Impacts of a Warming Arctic: Arctic Climate Impacts Assessment*, 1046 pp., Cambridge Univ. Press, Cambridge, U. K.

Jezek, K. C., M. R. Drinkwater, J. P. Crawford, R. Bindschadler, and R. Kwok (1993), Analysis of synthetic aperture radar data collected over the southwestern Greenland Ice Sheet, *J. Glaciol.*, *39*, 119–132.

Jezek, K. C., P. Gogineni, and M. Shanableh (1994), Radar measurements of melt zones on the Greenland Ice Sheet, *Geophys. Res. Lett.*, *21*, 33–36.

Kalnay, E., et al. (1996), The NCEP/NCAR 40-year reanalysis project, *Bull. Am. Meteorol. Soc.*, *77*, 437–471, doi:10.1175/1520-0477(1996)077<0437:TNYRP>2.0.CO;2.

Kaser, G., J. G. Cogley, M. B. Dyurgerov, M. F. Meier, and A. Ohmura (2006), Mass balance of glaciers and ice caps: Consensus estimates for 1961–2004, *Geophys. Res. Lett.*, *33*, L19501, doi:10.1029/2006GL027511.

Koerner, R. M. (1970), Some observations on superimposition of ice on the Devon Island Ice Cap, N. W. T., Canada, *Geogr. Ann.*, *52A*, 57–67.

Koerner, R. M. (1979), Accumulation, ablation, and oxygen isotope variations on the Queen Elizabeth Islands ice caps, Canada, *J. Glaciol.*, *22*, 25–41.

Koerner, R. M. (2002), Glaciers of the Arctic Islands, in *Satellite Image Atlas of Glaciers of the World. Glaciers of North America–Glaciers of Canada*, edited by R. S. J. Williams and J. G. Ferrigno, pp. 111–143, U.S. Geol. Surv., Washington, D. C.

Konig, M., J. Wadham, J. G. Winther, J. Kohler, and A. M. Nuttall (2002), Detection of superimposed ice on the glaciers Kongsvegen and midre Lovenbreen, Svalbard, using SAR satellite imagery, *Ann. Glaciol.*, *34*, 335–342.

Krabill, W. B., W. Abdalati, E. B. Frederick, S. S. Manizade, C. F. Martin, J. G. Sonntag, R. N. Swift, R. H. Thomas, and J. G. Yungel (2002), Aircraft laser altimetry measurement of elevation changes of the Greenland Ice Sheet: Technique and accuracy assessment, *J. Geodyn.*, *34*, 357–376, doi:10.1016/S0264-3707(02)00040-6.

Legresy, B., and F. Remy (1997), Altimetric observations of surface characteristics of the Antarctic Ice Sheet, *J. Glaciol.*, *43*, 265–275.

Lillesand, T. M., and R. W. Kiefer (1994), *Remote Sensing and Image Interpretation*, 3rd ed., 750 pp., John Wiley, New York.

Long, D. G., and M. R. Drinkwater (1994), Greenland Ice Sheet Surface-properties observed by the SEASAT-A scatterometer at enhanced resolution, *J. Glaciol.*, *40*, 213–230.

Long, D. G., and M. R. Drinkwater (1999), Cryosphere applications of NSCAT data, *IEEE Trans. Geosci. Remote Sens.*, *37*, 1671–1684, doi:10.1109/36.763287.

Long, D. G., and B. R. Hicks (2005), Standard BYU QuikSCAT/SeaWinds land/ice image products, report, Brigham Young Univ., Provo, Utah.

Long, D. G., P. J. Hardin, and P. T. Whiting (1993), Resolution enhancement of spaceborne scatterometer data, *IEEE Trans. Geosci. Remote Sens.*, *31*, 700–715, doi:10.1109/36.225536.

Marshall, S. J., M. J. Sharp, D. O. Burgess, and F. S. Anslow (2007), Near-surface temperature lapse rates on the Prince of Wales Icefield, Ellesmere Island, Canada: Implications for regional downscaling of temperature, *Int. J. Climatol.*, *27*, 385–398, doi:10.1002/joc.1396.

Massom, R., and D. Lubin (2006), *Ice Sheets*, vol. 2, 500 pp., Springer, Berlin.

Meier, M. F., M. B. Dyurgerov, U. K. Rick, S. O'Neel, W. T. Pfeffer, R. S. Anderson, S. P. Anderson, and A. F. Glazovsky (2007), Glaciers dominate Eustatic sea-level rise in the 21st century, *Science*, *317*, 1064–1067, doi:10.1126/science.1143906.

Nghiem, S. V., K. Steffen, G. Neumann, and R. Huff (2005), Mapping of ice layer extent and snow accumulation in the percolation zone of the Greenland Ice Sheet, *J. Geophys. Res.*, *110*, F02017, doi:10.1029/2004JF000234.

Nolin, A. W., and M. C. Payne (2007), Classification of glacier zones in western Greenland using albedo and surface roughness from the Multi-angle Imaging SpectroRadiometer (MISR), *Remote Sens. Environ.*, *107*, 264–275, doi:10.1016/j.rse.2006.11.004.

Østrem, G. (1975), ERTS data in glaciology—An effort to monitor glacier mass balance from satellite imagery, *J. Glaciol.*, *15*, 403–415.

Raper, S. C. B., and R. J. Braithwaite (2006), Low sea level rise projections from mountain glaciers and icecaps under global warming, *Nature*, *439*, 311–313, doi:10.1038/nature04448.

Scott, J. B. T., P. Nienow, D. Mair, V. Parry, E. Morris, and D. J. Wingham (2006), Importance of seasonal and annual layers in controlling backscatter to radar altimeters across the percolation zone of an ice sheet, *Geophys. Res. Lett.*, *33*, L24502, doi:10.1029/2006GL027974.

Sharp, M., and L. Wang (2009), A five-year record of summer melt on Eurasian Arctic ice caps, *J. Clim.*, *22*(1), 133–145.

Thomas, R., C. Davis, E. Frederick, W. Krabill, Y. H. Li, S. Manizade, and C. Martin (2008), A comparison of Greenland Ice Sheet volume changes derived from altimetry measurements, *J. Glaciol.*, *54*, 203–212, doi:10.3189/002214308784886225.

Thomas, R. H., W. Abdalati, E. Frederick, W. B. Krabill, S. Manizade, and K. Steffen (2003), Investigation of surface melting and dynamic thinning on Jakobshavn Isbrae, Greenland, *J. Glaciol.*, *49*, 231–239, doi:10.3189/172756503781830764.

Trenberth, K. E., et al. (2007), Observations: Surface and atmospheric climate change, in *Climate Change 2007: The Physical Science Basis. Contribution of Working Group I to the Fourth Assessment Report of the Intergovernmental Panel on Climate Change*, edited by S. Solomon et al., pp. 235–336, Cambridge Univ. Press, Cambridge, U. K.

Ulaby, F. T., and W. H. Stiles (1981), Microwave response of snow, *Adv. Space Res.*, *1*, 131–149, doi:10.1016/0273-1177(81)90389-6.

Wang, L., M. J. Sharp, B. Rivard, S. Marshall, and D. Burgess (2005), Melt season duration on Canadian Arctic ice caps, 2000–2004, *Geophys. Res. Lett.*, *32*, L19502, doi:10.1029/2005GL023962.

Wang, L., M. Sharp, B. Rivard, and K. Steffen (2007), Melt season duration and ice layer formation on the Greenland Ice Sheet, 2000–2004, *J. Geophys. Res.*, *112*, F04013, doi:10.1029/2007JF000760.

Williams, R. S., D. K. Hall, and C. S. Benson (1991), Analysis of glacier facies using satellite techniques, *J. Glaciol.*, *37*, 120–128.

Wingham, D. J. (1995), A method for determining the average height of a large topographic ice sheet from observations of the echo received by a satellite altimeter, *J. Glaciol.*, *41*, 125–141.

Wismann, V. R., and K. Boehnke (1996), Dramatic decrease in radar cross section over Greenland observed by the ERS-1 scatterometer between 1991 and 1995, in *IGARSS '96: 1996 International Geoscience and Remote Sensing Symposium: Remote Sensing for a Sustainable Future*, vol. 4, pp. 2014–2016, Inst. of Electr. and Electr. Eng., New York.

Zuo, Z., and J. Oerlemans (1997), Contribution of glacier melt to sea-level rise since AD 1865: A regionally differentiated calculation, *Clim. Dyn.*, *13*, 835–845, doi:10.1007/s003820050200.

Zwally, H. J., et al. (2002), ICESat's laser measurements of polar ice, atmosphere, ocean, and land, *J. Geodyn.*, *34*, 405–445, doi:10.1016/S0264-3707(02)00042-X.

M. Sharp and G. J. Wolken, Department of Earth and Atmospheric Sciences, University of Alberta, 1-26 Earth Sciences Building, Edmonton, AB T6G 2E3, Canada. (gwolken@ualberta.ca)

L. Wang, Climate Research Division, Atmospheric Science and Technology Directorate, Environment Canada, 4905 Dufferin Street, Toronto, ON M3H 5T4, Canada.